Optimal design of apodizing phase plate coronagraphs

Emiel H. Por

Leiden Observatory, Leiden University, P.O. Box 9513, 2300 RA Leiden, The Netherlands

ABSTRACT

Direct observations of exoplanets require a stellar coronagraph to suppress the diffracted starlight. An Apodizing Phase Plate (APP) coronagraph consists of a carefully designed phase-only mask in the pupil plane of the telescope. This mask alters the point spread function in such a way that it contains a dark zone at some off-axis region of interest, while still retaining a high Strehl ratio (and therefore high planet throughput).

Although many methods for designing such a phase mask exist, none of them provide a guarantee of global optimality. Here we present a method based on generalization of the phase-only mask to a complex amplitude mask. Maximizing the Strehl ratio while simultaneously constraining the stellar intensity in the dark zone turns out to be a quadratically constrained linear algorithm, for which a global optimum can be found using large-scale numerical optimizers. This generalized problem yields phase-only solutions. These solutions are therefore also solutions of the original problem.

Using this optimizer we perform parameter studies on the inner and outer working angle, the contrast and the size of the secondary obscuration of the telescope aperture for both one-sided and annular dark zones. We reach Strehl ratios of $> 65\%$ for a 10^{-5} contrast from 1.8 to $10\lambda/D$ with a one-sided dark zone for a VLT-like secondary obscuration. This study provides guidelines for designing APPs for more realistic apertures.

Keywords: high contrast imaging, coronagraphy, global optimization, design, apodizing phase plate

1. INTRODUCTION

For detecting Earth-like exoplanets, we need to overcome the huge contrast between planet and its host star. A coronagraph allows for separation of starlight and the light from its companion by suppressing the former and transmitting the latter. This suppression can be achieved by various types of optical systems.[1,2] One of these coronagraphic systems is known as the apodizing phase plate (APP), which consists of a single phase-only pupil-plane optic.[3] In this type of coronagraph, the starlight itself is not absorbed, but rather suppressed in a certain region of interest in the focal-plane known as the dark zone. The phase pattern on the pupil-plane element must therefore be designed to yield a point-spread function (PSF) that has extremely little light inside this dark zone.

Of course, the phase plate reduces the Strehl ratio of the star, as light is scattered out of the Airy core. Although we do not care about the Strehl ratio of the star, as the planet light is also incident on the same phase plate, its PSF is altered in the same way and its Strehl ratio is diminished by the same factor. We therefore need to simultaneously have a high Strehl ratio of the phase plate, while having the transmission inside the dark zone be extremely small.

We can therefore conclude that finding the phase pattern requires solving the following optimization problem:

$$\underset{\phi(x)}{\text{maximize}} \quad |E(0)|^2 \tag{1}$$

$$\text{subject to} \quad |E(k)|^2 \leq |E(0)|^2 \cdot 10^{-c} \; \forall \; k \in D \tag{2}$$

where $E(k)$ is the electric field in the focal plane, defined by

$$E(k) = \mathcal{F}\{A(x) \exp i\phi(x)\} \tag{3}$$

Correspondence: `por@strw.leidenuniv.nl`

and c is the contrast in the dark zone that we want to reach, $A(x)$ the telescope aperture, $\phi(x)$ the phase pattern in the pupil plane, x a position in the pupil plane, k a position in the focal plane, and D the dark zone in the focal plane. Note that there are many phase patterns that satisfy the constraint of contrast in the dark zone, however we want to select the phase pattern that simultaneously yields the highest planet throughput.

Solving this optimization problem is quite hard due to the non-linearity in the complex phase exponential. Previous methods have therefore not attempted to solve the full optimization problem, but rather to find a phase solution that is close to the global optimum. These algorithms often linearize the problem around a certain phase pattern and take small steps towards maximization of some merit function that includes both the planet throughput and contrast in the dark zone. This includes phase iteration techniques,[3,4] which were one of the first proposed methods for APP optimization, and modified Gerchberg-Saxton algorithms.[5] Due to the linearization involved in these optimization techniques, they will often get stuck in local optima and give no guarantee that they converge to a solution close to the optimal one. Additionally these algorithms do not constrain the intensity in the dark zone, but rather minimize that intensity without any regard for the set contrast limit.

Finding the global optimum has been previously attempted using general non-linear optimization methods such as simulated annealing. While these methods in theory provide the global optimum, they require vast amounts of computation time and only provide a guarantee of global optimality if given an infinite amount of computation time. Global optimization of shaped pupil coronagraphs[6] has been modified to optimize APPs,[7] however the resulting APPs contained only several discrete phase transitions, and were not globally optimal, as will be shown in this work. In this paper we slightly modify the approach of Carlotti et al.[7] and provide several improvements, both in speed and correctness at small inner working angles. We then present the fundamental limits of pupil-plane-only coronagraph designs, using parameter studies on simplified apertures using both one-sided and two-sided dark zones.

2. LINEARIZATION, DISCRETIZATION AND CORRECTION

2.1 Linearization

The linearization of the general optimization problem follows closely the work by Carlotti et al.,[7] but differs in a few key points. These will be indicated in the following derivation.

We first change the complex phase exponential to a complex function $X(x)+iY(x)$ where we require $X^2(x)+Y^2(x)=1$ and change optimization variables to finding the functions $X(x)$ and $Y(x)$. Note that this linearizes the calculation of $E(k)$ but does not change anything in the optimization problem: the non-linearity is now hidden in the constraints. The optimization problem now reads

$$\underset{X(x),Y(x)}{\text{maximize}} \quad |E(0)|^2 \tag{4}$$

$$\text{subject to} \quad |E(k)|^2 \le |E(0)|^2 \cdot 10^{-c} \ \forall \ k \in D \tag{5}$$

$$E(k) = \mathcal{F}\{A(x)(X(x)+iY(x))\} \tag{6}$$

$$X^2(x)+Y^2(x) = 1 \forall x. \tag{7}$$

To make the objective function linear, we can simply maximize the real value of $E(0)$ instead of its absolute value. While this may seem like an oversimplification, it only fixes the average phase of the pupil-plane phase pattern. Any other chosen phase (ie. optimizing for the imaginary part of $E(0)$ instead) can be obtained by multiplying the pupil-plane complex amplitude pattern by a constant complex phase exponential (ie. $\exp(i\pi/2)$ for the case mentioned above). This is possible as all constraints depend on the amplitude of some complex amplitude in the pupil or focal plane only and have no dependence on the phase of that quantity. The optimization problem now reads

$$\underset{X(x),Y(x)}{\text{maximize}} \quad \Re\{E(0)\} \tag{8}$$

$$\text{subject to} \quad |E(k)|^2 \le |E(0)|^2 \cdot 10^{-c} \ \forall \ k \in D \tag{9}$$

$$E(k) = \mathcal{F}\{A(x)(X(x)+iY(x))\} \tag{10}$$

$$X^2(x)+Y^2(x) = 1 \forall x. \tag{11}$$

The objective is now linear, and all constraints are convex and quadratic except for the constraint on the absolute value of the complex amplitude in the pupil-plane. To make this convex, we generalize the optimization problem to finding an optimal complex amplitude mask, instead of a phase-only mask. The new optimization problem does not guarantee phase-only solutions, however empirically this generalized optimization problem does yield phase-only solutions for all dark zone shapes, contrast limits and aperture geometries. Various examples of APP solutions for one-sided and two-sided dark zones, both for simple and complex aperture geometries, can be found in Figures 3 and 6. The optimization problem now reads

$$\underset{X(x),Y(x)}{\text{maximize}} \quad \Re\{E(0)\} \tag{12}$$

$$\text{subject to} \quad |E(k)|^2 \le |E(0)|^2 \cdot 10^{-c} \ \forall \ k \in D \tag{13}$$

$$E(k) = \mathcal{F}\{A(x)(X(x) + iY(x))\} \tag{14}$$

$$X^2(x) + Y^2(x) \le 1 \forall x. \tag{15}$$

This optimization problem is now convex and linear, and therefore has a unique global optimum which can be found using standard optimization techniques.

2.2 Discretization

To numerically optimize this optimization problem we have to discretize all functions. For simplicity, we discretize the focal and pupil plane into discrete set of points, $\{k_i\}$ and $\{x_i\}$ respectively. In this way calculation of the focal-plane electric field at those points can be done by a vector-matrix multiplication as

$$\mathbf{E}_{\text{foc}} = M\mathbf{E}_{\text{pup}}, \tag{16}$$

where $\mathbf{E}_{\text{foc}}$ is the focal-plane electric field at points $\{k_i\}$, $\mathbf{E}_{\text{pup}}$ the pupil-plane electric field at points $\{x_i\}$, and M the transformation matrix between pupil and focal plane.

The choice of the positions of discretization points in the focal plane is critical for correct performance. We always have discretization error: in between two points in the focal plane the PSF might actually exceed the contrast limit, while at the same time the PSF at the discretization points is within the limit. Due to computational time limitations we always want as little points in the focal plane as possible, while still covering the entire dark zone. In practice this works out to > 2 points per λ/D, corresponding to the Nyquist limit for the used aperture. For APPs with a high contrast (typically deeper than 10^{-6}) this is not enough, and we need ~ 3 points per λ/D. This is due to superoscillations[8,9] that occur in this regime: the electric field oscillates locally faster than the Nyquist rate of the aperture. This means that even if we constraint the electric field at > 2 points per Nyquist-limited period, the electric field will still vary within those points at an apparent spatial frequency higher than the Nyquist frequency itself. Constraining the electric field on more points bounds the strength of these superoscillations.[9]

2.3 Speed improvements

While a direct implementation of the above discretized optimization problem yields correct APPs, there are some changes that can be made to improve runtime and performance. In practice excluding the Strehl ratio from the dark zone constraint yields more than an order of magnitude shorter computation times. The reason for this can be attributed to the inner workings of the optimizer that was used.[10] Other optimizers may react differently. We replace actual Strehl ratio with the expected Strehl ratio of the optimization S_{expected}. The optimization problem now reads

$$\underset{X(x),Y(x)}{\text{maximize}} \quad \Re\{E(0)\} \tag{17}$$

$$\text{subject to} \quad |E(k)|^2 \le S_{\text{expected}} \cdot 10^{-c} \ \forall \ k \in D \tag{18}$$

$$E(k) = \mathcal{F}\{A(x)(X(x) + iY(x))\} \tag{19}$$

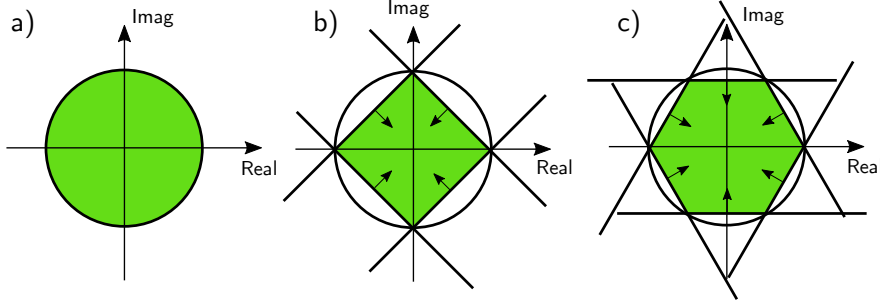$$X^2(x) + Y^2(x) \le 1 \forall x. \tag{20}$$

Figure 1. Rewriting square constraints to linear constraints can help computation times, while only having a small influence on the final Strehl ratio. *a)* A quadratic constraint contains all phase space but is computationally expensive. *b)* A box-shaped constraint consists of four linear constraints and balances coverage of the phase space, while keeping computation times in check. *c)* Higher-order regular polygons, such as this hexagon, require more linear constraints and therefore more computational resources, while yielding no significant improvement in the resulting Strehl ratios.

Note that to get a correct value for the Strehl ratio, we need to iterate this optimization multiple times, starting with $S_{\text{expected}}^{(0)} = 1$ and update the expected Strehl ratio after each optimization. In practice the Strehl ratio converges after $\sim 3 - 4$ iterations, except for extremely low Strehl ratios, in which we are not interested anyway.

Another improvement is the removal of quadratic constraints. These type of constraints are notoriously difficult for numerical optimizers and linear constraints are preferred. We can approximate the circle by an inscribed box as shown in Figure 1. Although this reduces the phase space of the optimization, in practice this doesn't reduce the Strehl ratio of the final APPs by much. Orienting the diagonal of the box in the direction of the unaltered electric field at that point in the focal plane increases the Strehl slightly and tends to reduce artifacts. The result of using a box-shaped constraint instead of a circular one is that the optimizer now prefers to put the final electric field in the direction of the diagonals. This also means that we cannot replace the pupil-plane quadratic constraints with box-shaped linear constraints: the optimized APP would consist of discrete phases (namely $0, \pi/2, \pi, 3\pi/2$). The discretized phases are precisely what Carlotti et al.[7] found. In the focal plane we do not care as much about the phase of the residual speckles and we can safely apply the box-shaped linear constraints. Using higher order regular convex polygons, such as the hexagon or octagon was found to yield a negligible improvement while significantly increasing computation time. The optimization problem now reads

$$\underset{X(x),Y(x)}{\text{maximize}} \quad \Re\{E(0)\} \tag{21}$$

$$\text{subject to} \quad \Re\{E(k)\} + \Im\{E(k)\} < \sqrt{S_{\text{expected}} \cdot 10^{-c}} \tag{22}$$

$$\Re\{E(k)\} - \Im\{E(k)\} < \sqrt{S_{\text{expected}} \cdot 10^{-c}} \tag{23}$$

$$-\Re\{E(k)\} + \Im\{E(k)\} < \sqrt{S_{\text{expected}} \cdot 10^{-c}} \tag{24}$$

$$-\Re\{E(k)\} - \Im\{E(k)\} < \sqrt{S_{\text{expected}} \cdot 10^{-c}} \tag{25}$$

$$E(k) = \mathcal{F}\{A(x)(X(x) + iY(x))\} \tag{26}$$

$$X^2(x) + Y^2(x) \leq 1 \forall x. \tag{27}$$

2.4 Tilt correction

When optimizing for small inner-working angle dark zones, we can often see that the core of the PSF is pushed away from the dark zone, effectively increasing the inner-working angle by that same amount: the core of the planet PSF is moved towards the star. This effect is commonly found in other APP optimization algorithms: introducing a tilt in the pupil-plane phase pattern and dealing with the reduced throughput of the core at $(0,0)$ is advantageous compared to suppressing the starlight that close to the PSF core. This is of course not desirable and we have to suppress this behavior in some way. Other optimizers deal with this by removing the introduced
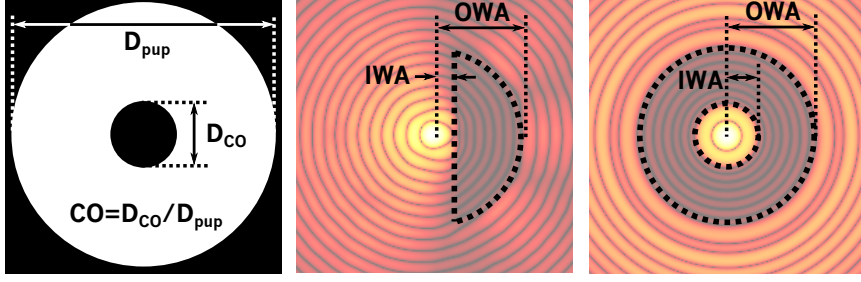
Figure 2. The pupil-plane and focal-plane geometry considered in this work. Any spiders holding up the central obscuration are neglected. *Left* The pupil of the telescope. *Middle* A D-shaped dark zone. *Right* An annular dark zone.

tilt each iterations (as in the case of the modified Gerchberg-Saxton algorithm) or by removing tip-tilt from the mode basis used for optimization. As we optimize electric field and have no access to the optimization algorithm directly, we instead have to introduce a constraint in the optimization problem to counteract this behavior.

The simplest and most effective way is to enforce that the PSF reaches its maximum at $(0,0)$. In this way moving the PSF is not allowed. This constraint can be approximated as a linear constraint by enforcing that the absolute value of both the real and imaginary part of the electric field may not be larger than its value at $(0,0)$. A quadratic constraint on the PSF itself would be best, but takes more computation time. Typically the PSF moves perpendicular to the dark zone shape, so we only need to enforce this in the direction opposite to the dark zone, starting at $(0,0)$ itself. The optimization problem now reads

$$\underset{X(x),Y(x)}{\text{maximize}} \quad \Re\{E(0)\} \tag{28}$$

$$\text{subject to} \quad \Re\{E(k)\} + \Im\{E(k)\} < \sqrt{S_{\text{expected}} \cdot 10^{-c}} \tag{29}$$

$$\Re\{E(k)\} - \Im\{E(k)\} < \sqrt{S_{\text{expected}} \cdot 10^{-c}} \tag{30}$$

$$-\Re\{E(k)\} + \Im\{E(k)\} < \sqrt{S_{\text{expected}} \cdot 10^{-c}} \tag{31}$$

$$-\Re\{E(k)\} - \Im\{E(k)\} < \sqrt{S_{\text{expected}} \cdot 10^{-c}} \tag{32}$$

$$E(k) = \mathcal{F}\{A(x)(X(x) + iY(x))\} \tag{33}$$

$$X^2(x) + Y^2(x) \leq 1 \forall x \tag{34}$$

$$\Re\{E(k)\} \leq \Re\{E(0)\} \forall k \tag{35}$$

$$-\Re\{E(k)\} \leq \Re\{E(0)\} \forall k \tag{36}$$

$$\Im\{E(k)\} \leq \Re\{E(0)\} \forall k \tag{37}$$

$$-\Im\{E(k)\} \leq \Re\{E(0)\} \forall k. \tag{38}$$

We use this final optimization problem for the rest of this paper.

3. CASE STUDIES

3.1 D-shaped dark zones

In this section we consider a D-shaped dark zone. This dark zone is parameterized by their inner-working angle, outer-working angle and contrast. For the aperture we take a circular aperture with a central obscuration. This geometry is shown graphically in Figure 2. In the following sections we vary the dark-zone parameters and use the Strehl ratio as a metric. In Figure 3 we show some solutions with their parameters along with the resulting PSF.
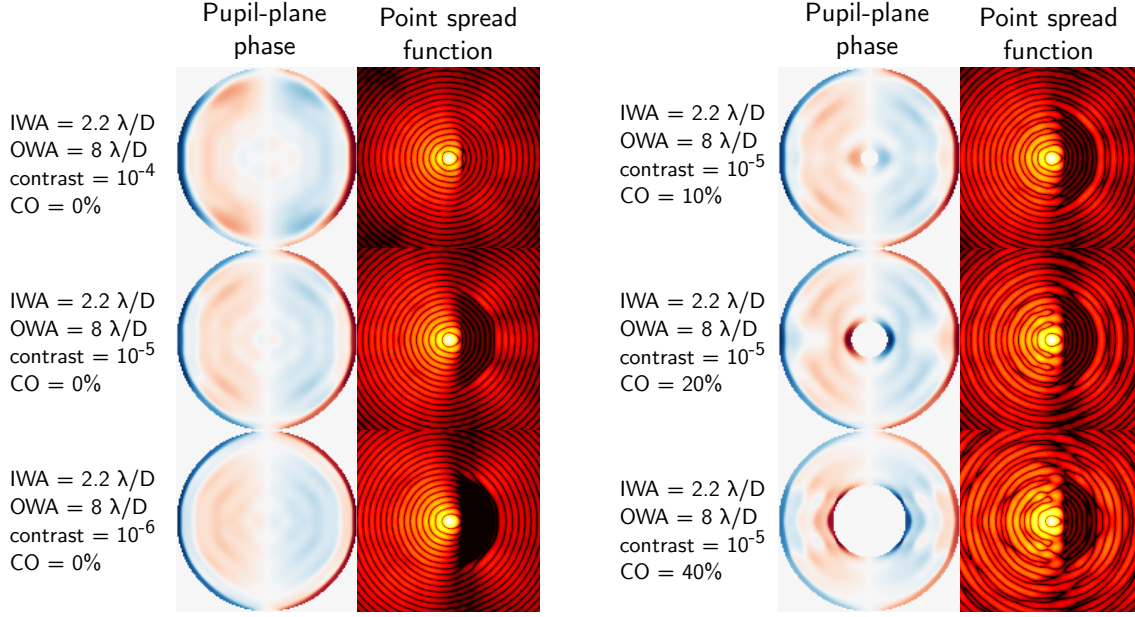
Figure 3. Some examples for optimization with D-shaped dark zones. For each set of input parameters, we show the final phase pattern and its corresponding point spread function.
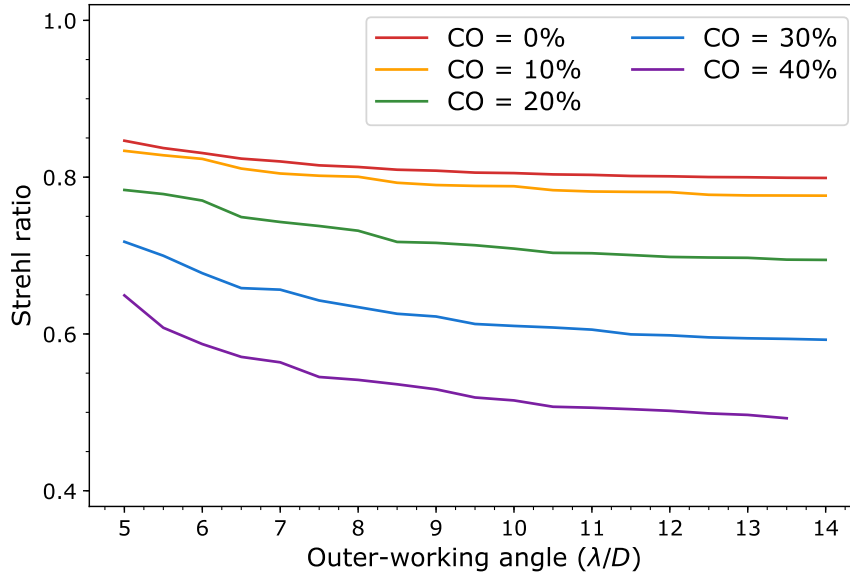

Figure 4. The Strehl ratio for a fixed inner-working angle ($2\lambda/D$) and contrast (10^{-5}) but varying outer-working angle for various values of the central obscuration CO. As the outer-working angle becomes larger, the Strehl ratio changes less and less. Outer-working angle is in these simulations limited by computation resources, both in memory and time.

3.1.1 Outer-working angle

We fix the inner-working angle at $IWA = 2\lambda/D$, the contrast at 10^{-5} and vary the outer-working angle and central obscuration. The Strehl ratio for these optimizations are shown in Figure 4. We can see that the Strehl ratio asymptotically converges to a fixed Strehl ratio for increasing outer-working angles. This suggests that designing infinite outer-working angle solutions might be feasible, and other optimization algorithms yield similar results.

3.1.2 Inner-working angle and contrast

The relation between the Strehl ratio S, inner-working angle and contrast paints a more complicated picture. We fix the outer-working angle at $8\lambda/D$ and vary the contrast and inner-working angle for various values of the central obscuration. The results of these optimization are shown in Figure 5. For an unobstructed aperture, the iso-Strehl lines generally have a constant gradient: if an APP is desired with a contrast 10 times deeper, the inner-working angle must be increased by $\sim 0.2\lambda/D$ to yield the same Strehl ratio. For the $S = 0.8$ line however, the gradient changes at $IWA = 1.6\lambda/D$ and a contrast of 10^{-4} to $\sim 0.5\lambda/D$ per decade in contrast. Introducing a 10% central obscuration, we can see that this turn-off point moves towards shallower contrasts. If we increase the central obscuration further, this trend continues and other iso-Strehls start to follow the same behavior.

Note that in these graphs, the increase in Strehl ratios at extremely low inner-working angles and high contrasts should not be trusted. These solutions tend to circumvent the tilt correction method described in Section 2.4 by producing a second peak beyond the range the tilt correction can protect against. This second peak is then the major contribution to Strehl ratio, while the peak at the origin $(0,0)$ still decreases.

3.2 Annular dark zones

Annular dark zones are generally easier to optimize, due to the symmetry that they provide. While symmetric optimization problems do not necessarily have symmetric solutions, see for example the excellent paper by Waterhouse,[11] in this case they do. The reasoning for this is simple. If a global optimum x has been found, the transformed solution $x' = T(x)$, where T is the transformation corresponding to a symmetry in the optimization problem, must also be a global optimum. In the case of a convex optimization problem where the objective function is strictly convex, the global optimum is unique. Therefore $x' = x$ and x must be a symmetric solution. As our optimization problem is convex with a strictly convex objective function, all symmetries in the system provide a symmetry of the solution.

This result can be applied to many symmetries. For example: when all focal-plane constraints are situated in points-symmetric positions around the origin (ie. a two-sided dark zone), the transformation $Y(x) \to -Y(x)$ is a symmetry of the optimization problem, as its corresponding focal-plane transformation is $E(k) \to \overline{E}(-k)$. Therefore, a global optimal solution for such a dark zone geometry must satisfy $Y(x) = -Y(x) = 0$, so the pupil-plane phase is real. Empirically we again find that the absolute value of the pupil-plane apodizer is maximized, so that $X(x) \in \{1, -1\}$. This simplification reduces all quadratic constraints to linear constraints, which makes the optimization problem a simple linear problem. This means that the APPs found by Carlotti et al.[7] were indeed globally optimal. An example of such an APP is shown in Figure 6.

Additionally, if the optimization problem is rotationally symmetric (ie. a rotationally symmetric pupil and dark zone), the solution must consist of rings of 0 or π in phase. Exploiting this symmetry leads to a significantly reduced computation time, and allows for extensive parameter studies.

3.2.1 Inner-working angle and contrast

We consider the case of a annular dark zone, parameterized by their inner working angle, outer working angle and contrast. As the aperture shape, we again use a circular aperture with a varying central obscuration size. This geometry is shown graphically in Figure 2. In Figure 7 we fix the contrast at 10^{-4} and vary the inner working angle, outer working angle and central obscuration. We show the Strehl ratio of the corresponding APP pattern. The most prominent feature of these graphs are the plateaus of almost equal Strehl ratio: for a wide range ($\sim 1\lambda/D$) in both inner and outer working angles, the Strehl does not vary significantly. This is not an artifact of the optimization method but rather is related to the structure of the Airy rings of the unaltered telescope PSF. The Strehl depends on the number of Airy rings that need to be suppressed, rather than the total area of the dark zone.

The transitions between the plateaus do not correspond directly to the center of an Airy ring, but the plateaus are slightly broader. This can be attributed to the Airy ring being 'compressed' more easily than being suppressed entirely. Also note that the transition from good Strehl ($\gtrsim 50\%$) to bad Strehl ($\lesssim 10\%$) is extremely steep in inner working angle, and becomes steeper when the central obscuration is larger. The reason for this is the relative strength of the first Airy ring compared to the Airy core, which rises when the central obscuration
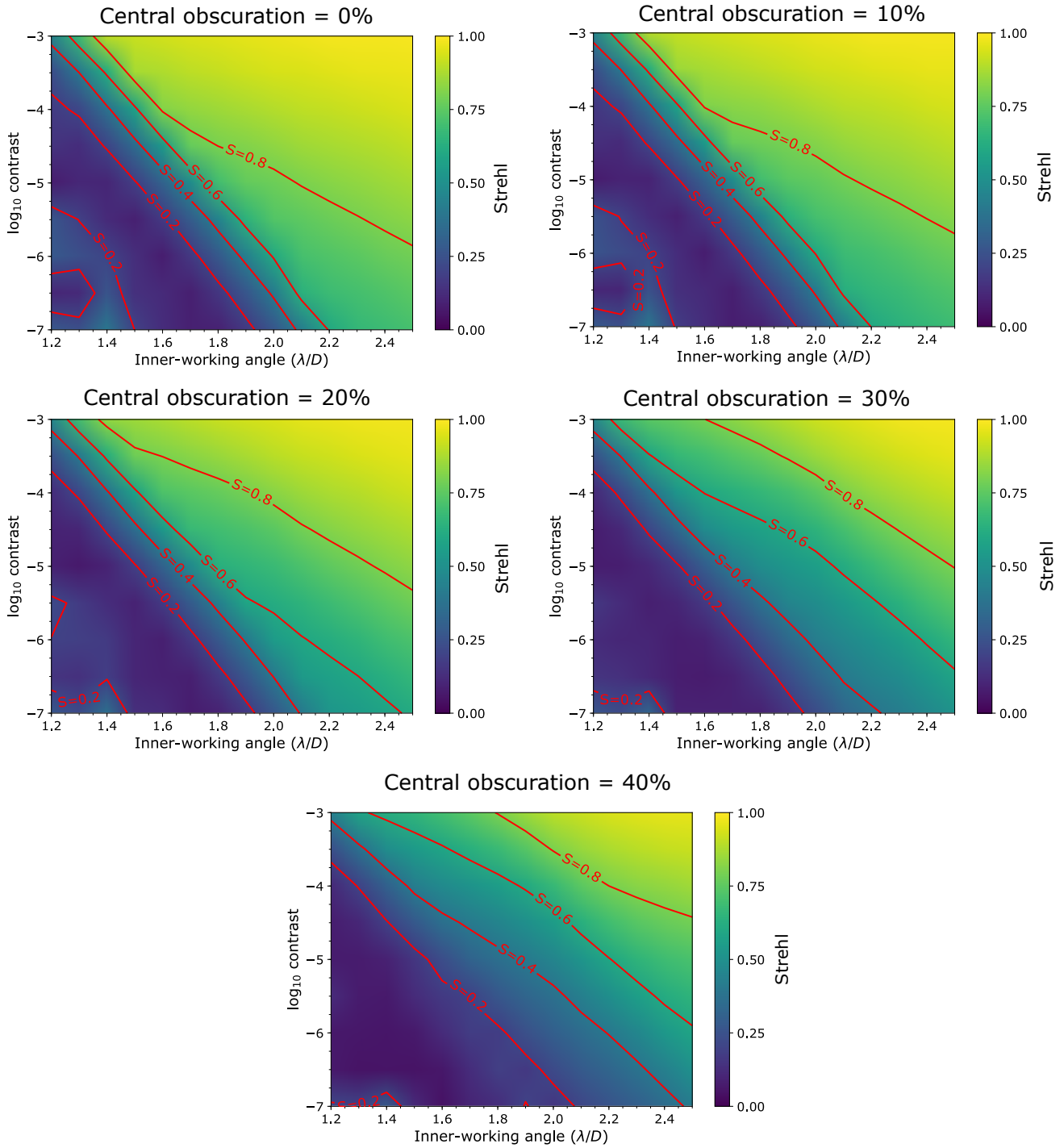
Figure 5. The Strehl ratio as a function of inner working angle, contrast and central obscuration size for a D-shaped dark zone. The outer working angle was fixed at $8\lambda/D$. See the text for a qualitative description of all features visible in this figure. These graphs can be used as a starting point for designing an APP for more complicated apertures.
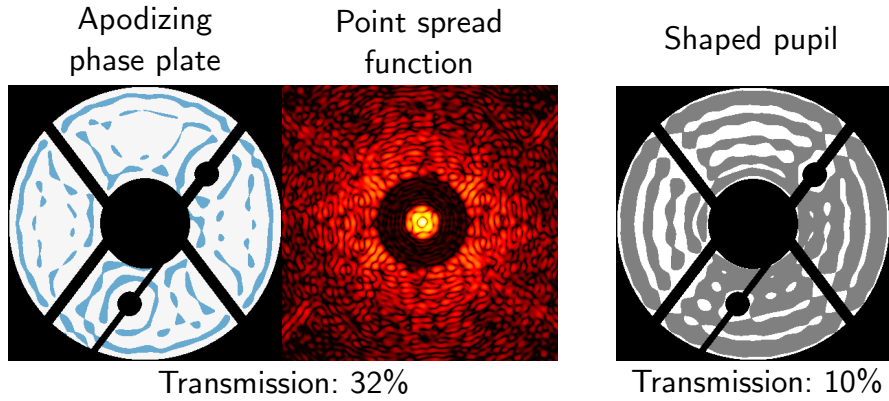
Apodizing phase plate   Point spread function   Shaped pupil

Transmission: 32%   Transmission: 10%

Figure 6. An example of a 360 APP for a complicated aperture. This aperture, based on the Subaru pupil, contains a large central obscuration, spiders, and masked dead deformable mirror actuators. A shaped pupil design for the same dark-zone geometry is also shown. As the phase space for shaped pupils is completely contained in the phase space allows in the APP optimizations, the transmission of the shaped pupil will always be lower than the optimized APP.
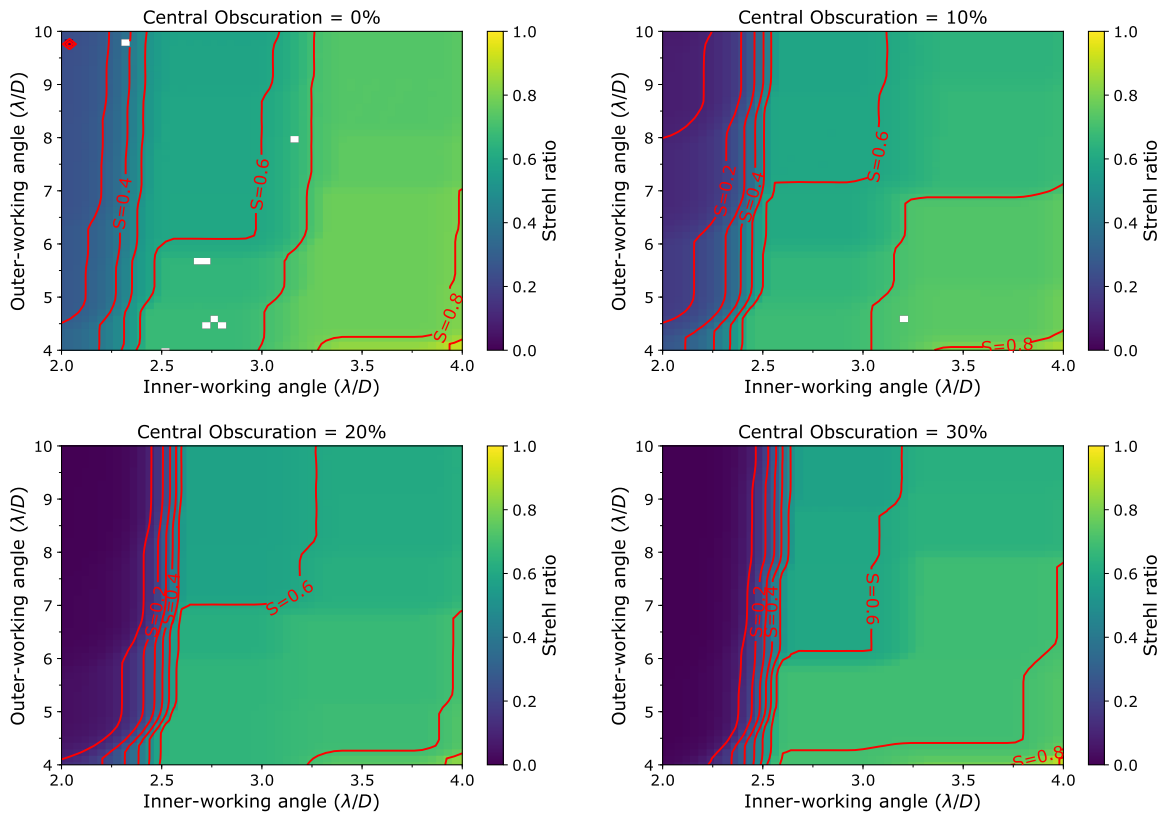

Figure 7. A parameter study on inner and outer working angle and central obscuration for annular dark zones. The contrast was fixed at 10^{-4}. The most prominent features are the existence of plateaus of equal Strehl ratio. These are determined by the positions of the original position of the Airy rings. A qualitative discussion can be found in the text.
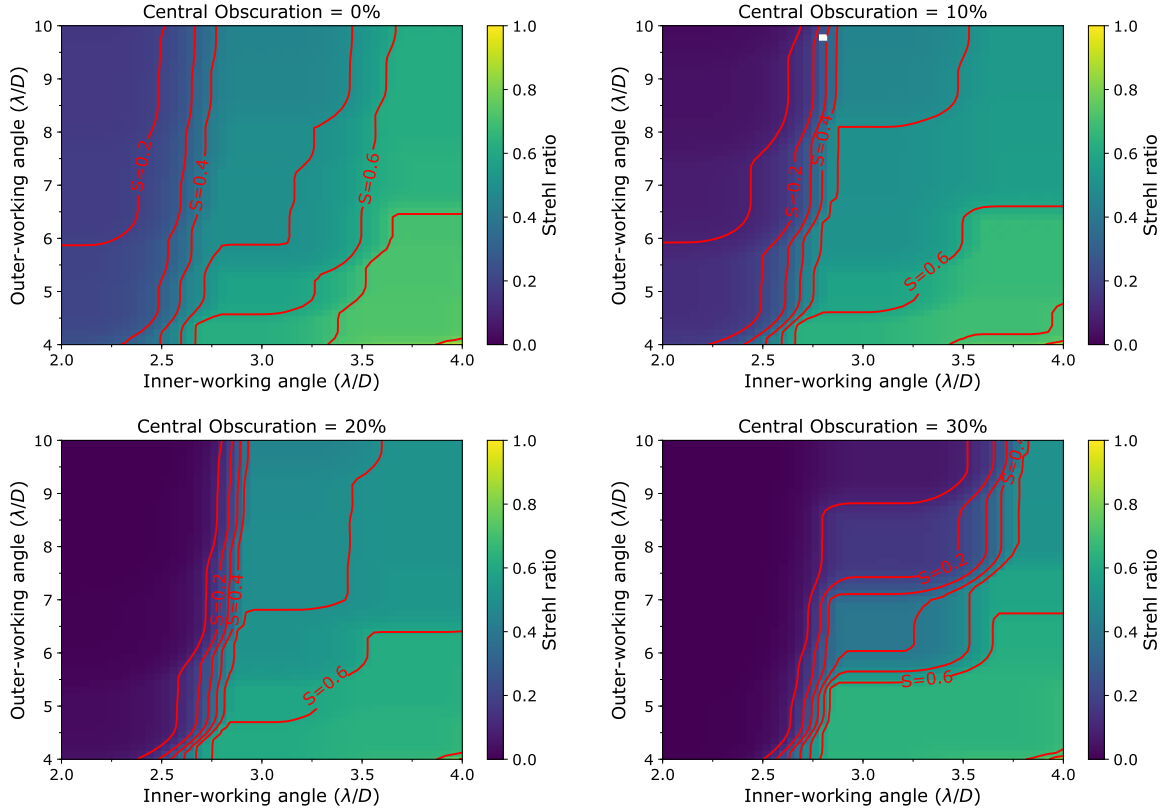
Figure 8. Identical to Figure 7 except for the changed contrast to 10^{-5}.

is enlarged. In addition, the Airy ring also moves outwards with larger central obscurations. This means that more Strehl needs to be expended to suppress that Airy ring, as the Strehl is correlated with the amount of light that needs to be suppressed, rather than the suppressed area.

In Figure 8 we show the same results as in Figure 7, but fix the contrast to 10^{-5}. The general behavior is similar to Figure 7. All effects mentioned above are however much more visible due to the deeper contrast requirements. For example, for a 30% central obscuration, the transition between good and bad Strehl even extends towards the third Airy ring.

3.2.2 Large outer-working angles

While the case for large outer working angles for D-shaped APPs was limited to $\sim 14\lambda/D$ due to computer memory limitations, for the circularly symmetric case we can go much further than that. In Figure 9 we show an example solution for a $100\lambda/D$ outer working angle. In this example, the inner-working angle was $3.5\lambda/D$, the contrast 10^{-5} and the central obscuration 10%. The optimized APP had a Strehl ratio of $S = 40\%$. The solution again consists of many rings of 0 or π phase. We can see that the width of the rings changes smoothly over the aperture, being wide at the edge and at the center of the aperture, while vanishing in between. This suggests, and this is confirmed by other 360 APP optimizations, that the size of the rings, and therefore their spacing, is dependent on the outer working angle, and their width is modulated by a spatial frequency determined by the inner working angle.

In the PSF we can see that the APP pushes the light into a ring just outside of the outer working angle. In the dark zone, many rings are visible, each with a maximum contrast of 10^{-5}. We can therefore see that if we keep increasing the outer working angle, this ring of light will be evenly distributed over the dark zone and eventually we will run out of light. At that point the contrast outside of the outer working angle will also
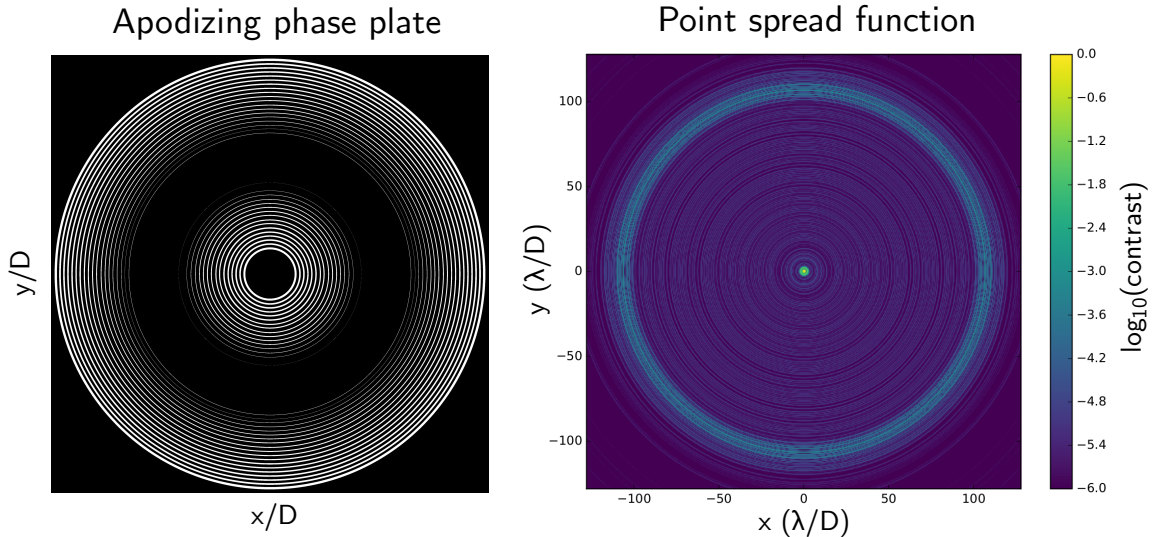
Figure 9. An example of an APP with a annular dark zone and an extremely large outer working angle of $100\lambda/D$. Other parameters were an inner working angle of $3.5\lambda/D$, a contrast of 10^{-5} and a central obscuration of 10%. The Strehl ratio was 40%.

be smaller than the required contrast and we will have obtained an infinite outer working angle APP with an annular dark zone.

4. CONCLUSIONS

We have shown a new method for optimizing apodizing phase plate coronagraphs. This method, based on the work by Carlotti et al.,[7] uses a convex linearized version of the full optimization problem, which can be globally optimized using large-scale linear optimizers. While this optimization problem in theory allows for amplitude apodization, in practice all solutions turn out to have unit amplitude, making them phase-only pupil-plane apodizers. We performed parameter studies for one-sided D-shaped and two-sided annular dark zones. These simulations serve as a starting point for a parameter study for realistic, more complicated apertures. Additionally, we showed that globally optimized two-sided APPs contain only 0 or π phase.

Future research will apply this optimizer to the optimization of pre-apodizers for phase-mask coronagraphs, such as the vortex[5,12] or the four-quadrant phase-mask coronagraph.[12] Similar pre-apodizers can most likely be found for apodized Lyot coronagraphs.[13,14]

ACKNOWLEDGMENTS

REFERENCES

[1] Guyon, O., Pluzhnik, E., Kuchner, M., Collins, B., and Ridgway, S., "Theoretical limits on extrasolar terrestrial planet detection with coronagraphs," *The Astrophysical Journal Supplement Series* **167**(1), 81 (2006).

[2] Mawet, D., Pueyo, L., Lawson, P., Mugnier, L., Traub, W., Boccaletti, A., Trauger, J. T., Gladysz, S., Serabyn, E., Milli, J., et al., "Review of small-angle coronagraphic techniques in the wake of ground-based second-generation adaptive optics systems," in [*SPIE Astronomical Telescopes+ Instrumentation*], 844204–844204, International Society for Optics and Photonics (2012).

[3] Codona, J., Kenworthy, M., Hinz, P., Angel, J., and Woolf, N., "A high-contrast coronagraph for the mmt using phase apodization: design and observations at 5 microns and 2 λ/d radius," in [*SPIE Astronomical Telescopes+ Instrumentation*], 62691N–62691N, International Society for Optics and Photonics (2006).

[4] Codona, J. L. and Angel, R., "Imaging extrasolar planets by stellar halo suppression in separately corrected color bands," *The Astrophysical Journal Letters* **604**(2), L117 (2004).

[5] Ruane, G. J., Huby, E., Absil, O., Mawet, D., Delacroix, C., Carlomagno, B., and Swartzlander, G. A., "Lyot-plane phase masks for improved high-contrast imaging with a vortex coronagraph," *Astronomy & Astrophysics* **583**, A81 (2015).

[6] Carlotti, A., Vanderbei, R., and Kasdin, N., "Optimal pupil apodizations of arbitrary apertures for high-contrast imaging," *Optics Express* **19**(27), 26796–26809 (2011).

[7] Carlotti, A., Kasdin, N. J., Vanderbei, R. J., and Riggs, A. E., "Hybrid coronagraphic design: optimization of complex apodizers," in [*SPIE Optical Engineering+ Applications*], 88641Q–88641Q, International Society for Optics and Photonics (2013).

[8] Aharonov, Y., Anandan, J., Popescu, S., and Vaidman, L., "Superpositions of time evolutions of a quantum system and a quantum time-translation machine," *Physical review letters* **64**(25), 2965 (1990).

[9] Ferreira, P. J. and Kempf, A., "Superoscillations: faster than the nyquist rate," *IEEE transactions on signal processing* **54**(10), 3732–3740 (2006).

[10] Gurobi Optimization, I., "Gurobi optimizer reference manual," (2016).

[11] Waterhouse, W. C., "Do symmetric problems have symmetric solutions?," *The American Mathematical Monthly* **90**(6), 378–387 (1983).

[12] Carlotti, A., Pueyo, L., and Mawet, D., "Apodized phase mask coronagraphs for arbitrary apertures-ii. comprehensive review of solutions for the vortex coronagraph," *Astronomy & Astrophysics* **566**, A31 (2014).

[13] NDiaye, M., Soummer, R., Pueyo, L., Carlotti, A., Stark, C. C., and Perrin, M. D., "Apodized pupil lyot coronagraphs for arbitrary apertures. v. hybrid shaped pupil designs for imaging earth-like planets with future space observatories," *The Astrophysical Journal* **818**(2), 163 (2016).

[14] Zimmerman, N. T., Riggs, A. E., Kasdin, N. J., Carlotti, A., and Vanderbei, R. J., "Shaped pupil lyot coronagraphs: high-contrast solutions for restricted focal planes," *Journal of Astronomical Telescopes, Instruments, and Systems* **2**(1), 011012–011012 (2016).